Polymer 50 (2009) 524–533

Contents lists available at ScienceDirect

Polymer

journal homepage: www.elsevier.com/locate/polymer

Rheological investigations of linear and hyperbranched polyethersulfone towards their as-spun phase inversion membranes' differences

Qian Yang [a], Tai-Shung Chung [a,*], M. Weber [b], K. Wollny [c]

[a] Department of Chemical and Biomolecular Engineering, National University of Singapore, Singapore 119260, Singapore
[b] Polymer Research Engineering Plastics, BASF SE, GKT/B-B1, Ludwigshafen 67056, Germany
[c] Anton Paar Germany GmbH, Stuttgart, HRB 214459, Germany

ARTICLE INFO

Article history:
Received 25 July 2008
Received in revised form
4 November 2008
Accepted 14 November 2008
Available online 30 November 2008

Keywords:
Polyethersulfone
Polymer processing
Polymer rheology

ABSTRACT

We have investigated the macromolecular structure and rheological behavior of both linear and hyperbranched polyethersulfone (PES) materials. It was found that the hyperbranched PES material has a higher molecular weight and a wider molecular weight distribution than its linear analogue. Rheological studies disclose that polymer solutions made from the HPES/polyvinylpyrrolidone (PVP)/*N*-methyl-2-pyrrolidone (NMP) ternary system have a longer relaxation time than their linear counterparts. The less relaxation characteristics of the HPES dope not only result in a more pronounced die swelling during hollow fiber spinning, but also produce hollow fiber membranes with smaller pore sizes, narrower pore size distribution, and a smaller molecular weight cut-off (MWCO). In addition, elongational viscosity characterizations indicate that HPES possesses a more strain hardening effect than LPES. As a result, films made from the former tends to break easier and quicker under high extensional strains than those made from the latter.

1. Introduction

Over the last few decades, synthetic polymeric membranes made from linear polyethersulfone (LPES) materials have been widely used for microfiltration, ultrafiltration, gas separation and many other separation applications. Among these applications, the LPES material has emerged as the most popular material for the fabrication of kidney dialysis membranes via phase inversion process due to its excellent stability under sterilization, superior biocompatibility after chemical modification, minimal degradation in dialysis performance over extended period of time, and easy fabrication [1–3]. Polymers with hyperbranched structure have also witnessed gaining interests recently due to their unique functional groups, high surface reactivity, and potentially greater biocompatibility in contrast to their linear analogues [4–6]. The knowledge of various synthetic approaches and characterization methods for hyperbranched polymers has been well established. However, the fundamental study of the relationship among material chemistry, physiochemical properties, membrane formation, and separation performance of these hyperbranched polymers is still in infancy [7].

Generally, the hyperbranched polymers possess intrinsic higher solubility, lower melt or solution viscosity that favor easy spinning [8] and enhance manufacturing throughput. The purposes of this study are to explore the rheology of LPES and HPES polymer materials as well as their polymeric solutions, and to identify the effects of hyperbranched structure on membrane's formation and macromolecular morphology. A comprehensive rheology study on both molten LPES and HPES materials was firstly conducted to characterize their macromolecular structure in terms of molecular weight, polydispersity, molecular entanglement, etc. Then rheological investigations were carried out for both polymers in their solution forms in order to correlate the relationship among their rheolog-ical characteristics, membrane morphologies and separation performance.

2. Experimental

2.1. Materials

Linear polyethersulfone (Ultrason® E6020P, Ultrason is a registered trademark of BASF SE) with 100 mol% linear unit and hyperbranched polyethersulfone with 2 mol% branched unit and 98 mol% linear unit (thereafter abbreviated as LPES and HPES, respectively) were kindly supplied by BASF Company, Germany. The chemical structures of both linear and branched polyethersulfone units were provided by BASF Company and are shown

* Corresponding author. Department of Chemical and Biomolecular Engineering, National University of Singapore, 10 Kent Ridge Crescent, Singapore 119260, Singapore. Tel.: +65 6874 6645; fax: +65 6779 1936.
E-mail address: chencts@nus.edu.sg (T.S. Chung).

0032-3861/$ – see front matter © 2008 Elsevier Ltd. All rights reserved.
doi:10.1016/j.polymer.2008.11.039

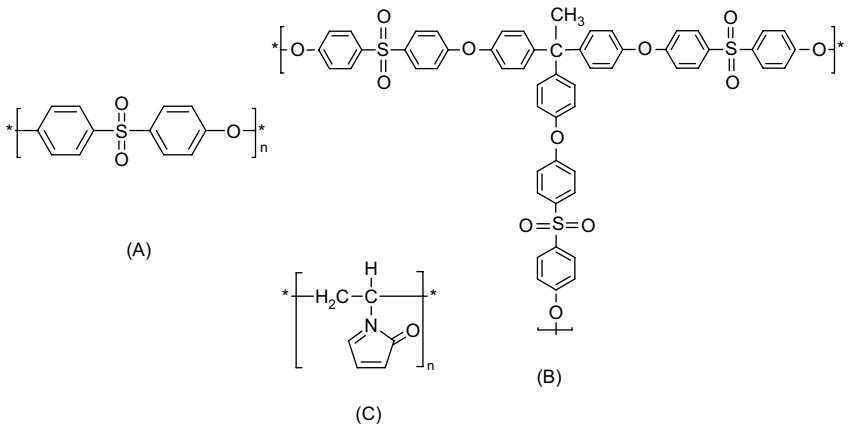

Fig. 1. The chemical structures of (A) linear polyethersulfone (LPES) unit, (B) hyperbranched polyethersulfone (HPES) unit and (C) polyvinylpyrrolidone (PVP).

in Fig. 1. *N*-Methyl-2-pyrrolidone (NMP) and dichloromethane (CH_2Cl_2) (Merck, Singapore) as the solvents, isopropanol (IPA) (Merck, Singapore) as the non-solvent and polyvinylpyrrolidone (PVP) (Merck, Singapore) with an average M_w of 360 kDa as an additive were employed for hollow fiber kidney dialysis membrane spinning. Polyethyleneglycol (PEG) (Aldrich, Singapore) with molecular weights from 600 up to 35,000 Da was used as model solutes to measure the ultrafiltration separation performance for the as-spun hollow fiber membranes. Methanol (Merck, Singapore) and *n*-hexane (Merck, Singapore) were utilized to conduct solvent exchange for as-spun hollow fiber membranes.

2.2. Preparation of membrane films

For dynamic mechanical analyses (DMAs), dense membrane films were prepared as follows: thin LPES or HPES films (30–50 μm) were cast from 2 wt% HPES or LPES in CH_2Cl_2 solutions, respectively on a silicon wafer at room temperature for 4–5 days. The resultant films were further dried under vacuum with temperature gradually increased to 250 °C and then held for another 1–2 days to remove any residual solvents.

For extensional viscosity (η_u) measurements, asymmetric membrane films were prepared as follows: the dried LPES or HPES polymers were completely dissolved in NMP to make a final composition of 32 wt%. The polymer solutions were degassed overnight before casting onto a glass plate by a ~280 μm thick casting knife. The nascent films were immediately immersed into a water bath and left overnight. The films were then immersed in fresh methanol for three times with half an hour each and continued with fresh hexane immersing within the same period of time to remove water and residual solvents. After solvent exchange, the membranes were dried naturally in the air.

2.3. Thermal characterizations of LPES and HPES polymer materials

The decomposition temperatures (T_ds) of dried LPES and HPES granules were determined using a Thermo-Gravimetric Analysis (TGA, TA Instruments version 2050) at 5% weight loss. The DMAs for LPES and HPES dense films were performed with DMA2980 from TA instruments. One rectangular slice from LPES or HPES dense films was loaded in a tension-film clamp, respectively and heated from −80 °C to 270 °C at a heating rate of 3 °C/min with a frequency of 1 Hz and an amplitude of 20 μm. The loss tangent (tan δ) peak temperature was chosen for both polymer materials as the preferred indicator of glass transition temperature (T_g). These thermal properties were essential for the subsequent rheology tests.

2.4. Rheological characterizations of LPES and HPES polymeric materials

To characterize LPES and HPES macromolecular structures, their rheological properties at the molten state were obtained using a Physica Rheometer (Model: MCR 501, Anton Paar, Germany) with a convection temperature device (Model: CTD 450, Anton Paar, Germany) consisting of a thermostat chamber equipped with a thermosensor. Parallel-plate geometry fixtures with a diameter of 25 mm were chosen for the steady shear rotation and dynamic frequency sweep tests. The granular LPES or HPES polymer material was placed onto the lower plate and heated to 370 °C inside the convection device. The measuring cell was purged with nitrogen gas as inert atmosphere to avoid the degradation of the molten samples. Approximately two minutes later the polymer granules were molten and tested. Special care has to be taken to avoid air bubbles during tests. Finally, the measuring position of 0.75 mm between two parallel plates was established.

Within the linear viscoelastic range, a strain of 10% was chosen for frequency sweep tests at various temperatures with angular frequency varying from 0.1 s^{-1} to 628 s^{-1}. The time–temperature–superposition (TTS) technique was applied so that all curves were shifted towards a predefined reference temperature to obtain the master curve that covers a much wider frequency range up to ~100,000 rad/s compared to a single frequency sweep. A flow curve was then derived from the frequency sweep data utilizing the master curve via the empirical Cox–Merz rule [9–12] in which the shear rate ($\dot{\gamma}$) dependence of the steady state shear viscosity (η) is equal to the angular frequency (ω) dependence of the complex viscosity (η^*) as follows:

$$\eta^*(\omega) = \eta(\dot{\gamma}) \quad \text{with } \omega = \dot{\gamma} \tag{1}$$

The Carreau–Yasuda regression [13] was then applied to the above flow curve of shear viscosity vs. shear rate to obtain

Table 1
Experimental parameters for hollow fiber membrane spinning.

Dope solution composition	Polymer/PVP/NMP (16/10/74 wt%)
Dope flow rate (ml/min)	2
Internal coagulant	NMP/water (55/45 wt%)
Bore flow rate (ml/min)	1.5
Length of air gap (cm)	20
External coagulant	IPA (1st), tap water (2nd)
Spinneret dimensions (mm)	0.86/0.5 (OD/ID)
Length of capillary channel (mm)	30
Spinning temperature (°C)	26
Spinning humidity (%)	60
Take-up speed (m/min)	5.16 (free falling)

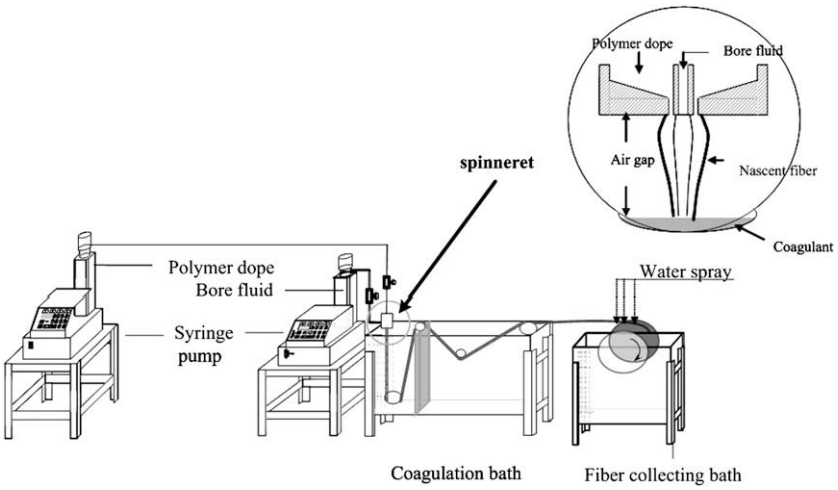

Fig. 2. Schematic of hollow fiber kidney dialysis membrane spinning process via dry-jet wet phase inversion approach.

additional rheological parameters such as power law exponent (n), relaxation time (λ), and width of transition (a) from the Newtonian to Non-Newtonian flow behavior.

$$\eta = (\eta_0 - \eta_\infty)\left[1 + (\lambda\dot{\gamma})^a\right]^{\frac{n-1}{a}} + \eta_\infty \quad (2)$$

The RheoPlus software package (Version 3.11, Anton Paar, Germany), the latest sophisticated molar mass distribution (MMD) method, was utilized to calculate molecular weight (M_w) and polydispersity index (PDI) of LPES and HPES based on data from frequency sweep tests, zero-shear viscosity and crossover point.

Furthermore, a film fixture was chosen for performing the extensional viscosity (η_u) measurements on LPES and HPES asymmetric flat membranes at a constant extensional rate of 0.001 s^{-1} and at an isotherm temperature of 150 °C.

The rheological properties of both LPES and HPES polymeric solutions were also performed using an Advanced Rheometric Expansion System (ARES) (Rheometric Scientific, USA) using a 25 mm cone-and-plate fixture with a cone angle at 0.04 rad. Firstly, the dynamic frequency sweep tests were conducted on polymer ternary systems of polymer/PVP/NMP (16/10/74 wt%), the typical compositions for dialysis membrane spinnings [14,15]. A strain of 1% was chosen for frequency sweep tests within the linear viscoelastic range with angular frequency varying from 0.1 s^{-1} to 100 s^{-1}. Thixotropy tests, the time dependent flow behavior for both polymer solutions, were then conducted with a loop shear rate from 0 → 50 → 0 s^{-1}, each segment for 5 min. The resulting curves were used to evaluate the hysteresis and relaxation performances for both polymer solutions after a progressively changed shear rate. Both tests were conducted at 25 °C provided by a thermostat oven.

To further investigate the rheology and temperature dependence of both polymer solutions, alternative measurements on zero-shear viscosity were conducted as follows: A series of dynamic frequency sweep tests were conducted at different temperatures with a constant shear strain of 1% within the linear viscoelastic region. Within the small amplitude oscillatory tests, the zero-shear viscosity η_0 was determined by the characteristic modulus (G_c) and the characteristic frequency (ω_c) at the crossover point (COP) as follows [16,17]:

$$\eta_0 = \frac{G_c}{2\pi\omega_c} \quad (3)$$

2.5. Fabrications of hollow fiber membranes and modules' preparation for ultrafiltration tests

Asymmetrical hollow fibers were spun from LPES and HPES polymer solutions at a composition of 16/10/74 wt% polymer/PVP/NMP by the dry-jet wet spinning process with detailed spinning conditions listed in Table 1. The schematic of hollow fiber spinning process is shown in Fig. 2 and more details have been described elsewhere [14,15]. The produced fibers were firstly contacted with bore fluid as well as air at an air-gap distance of 20 cm before immersed in the external coagulation bath. The external dual-coagulation bath was filled with IPA first followed by tap water. All nascent fibers were not drawn, that is, the take-up velocity (5.16 m/min) of the hollow fiber membrane was nearly the same as the free falling velocity in the coagulation bath. The nascent fibers exiting from the spinneret were snapshot by a Canon EOS 350D digit camera equipped with a microlens. Initial dimensions at a die swell range were measured in pixel value by an image processing software package (Image-Pro Plus 6.0, Media Cybernetics Inc.). The die swelling ratio was defined as the ratio of the biggest outer diameter of the nascent fiber to the outer diameter of the extrudate exiting from the spinneret.

The resultant fibers were solvent exchanged and freeze dried in a Thermo Savant ModulyoD freeze dryer (Thermo Electron Corp., USA) for membrane module assembling. Each module was tested from an in-to-out (i.e., from the lumen to the shell side) mode by an ultrafiltration unit in terms of pure water permeation flux (PWP) and solute separation performance at a trans-membrane pressure of about 8×10^4 Pa (gauge) (0.8 bar) at room temperature. The normalized pure water permeation flux (PWP, L/m^2/bar/h) was calculated by the following equation:

Table 2
Summary of LPES and HPES polymer materials' properties.

Polymers	Molecular weight (M_w)	Polydispersity index (PDI)	T_g (°C)	T_d at 5% weight loss (°C)	Zero-shear viscosity (η_0, Pa s)	Relaxation time (λ, s)	Width of transition range (a)	Power law exponent (n)
LPES	207,000	2.293	244.92	526.85	5650	0.0093	0.5136	1.0001
HPES	529,000	3.331	238.47	579.72	–	1.1834	0.1942	1.1748

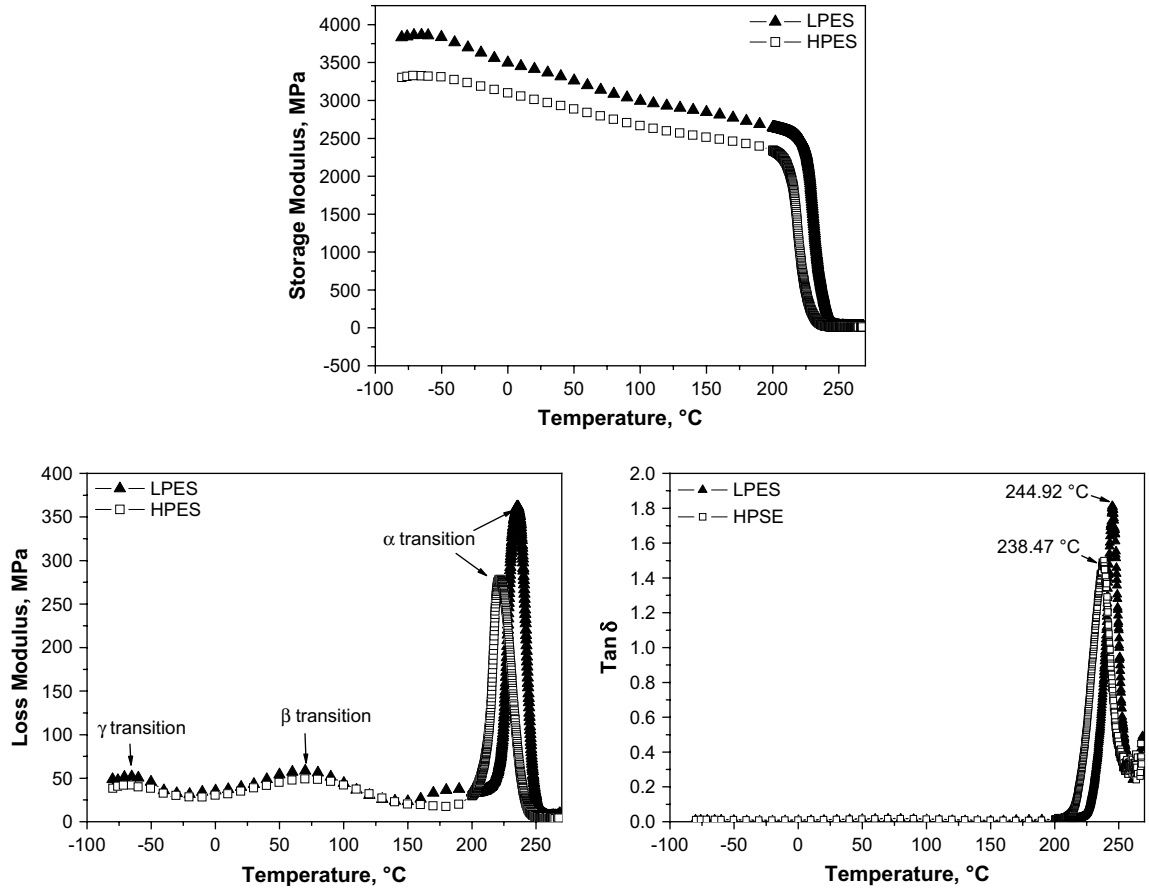

Fig. 3. The DMA diagrams for LPES and HPES dense films.

$$\mathrm{PWP} = \frac{Q}{A\Delta P} \tag{4}$$

where Q is the permeate volume in a predetermined time period (L/h), A is the effective membrane inner surface area (m^2), ΔP is the trans-membrane pressure (bar).

After the pure water permeation test, the pore size distribution of the membrane was characterized by gradually increasing molecular weights of the PEG solutes. The feed PEG concentration was around 200 ppm to minimize the occurrence of concentration polarization. Based on the obtained solute rejection data, the mean effective pore size (μ_p) equal to the diameter corresponding to 50% of solute rejection, the geometric standard deviation (σ_p) determined from the ratio of diameters corresponding to 84.13% and 50% rejections, the molecular weight cut-off (MWCO) corresponding to 90% salt rejection, and the pore size (d_p) distribution can be obtained according to the solute rejection approach [18–22].

2.6. SEM and AFM characterizations of the hollow fiber membranes

For the morphological study, fiber samples were immersed in liquid nitrogen and fractured. The cross-sections of the inner layer (IL, close to the fiber's lumen), outer layer (OL, close to the fiber's shell), inner surface (IS) and outer surface (OS) of the freeze-dried fibers were sputtered with platinum using a JEOL JFC-1300 platinum coater and then observed under a JEOL JSM-6700F Field Emission Scanning Electron Microscope (FESEM).

Atomic force microscopic (AFM) studies were conducted at the inner surface (IS) and outer surface (OS) of the hollow fibers also in their dry conditions using a Nanoscope IIIA AFM (Digital Instruments Inc., USA). Both inner and outer surfaces were exposed by cutting the fibers open and fixed to a metal disk by a double-sided tape. A crystal silicone probe cantilever was utilized in a tapping mode and the scanning area of each sample was 5 μm × 5 μm.

2.7. Measurements of mechanical strengths of hollow fiber membranes

Tensile properties of as-spun hollow fiber membranes were measured using an Instron test unit (INSTRON 5542 model). All the fiber samples were measured at a 50 mm gauge length with an elongation speed of 50 mm/min. At least five fiber samples were tested for each datum.

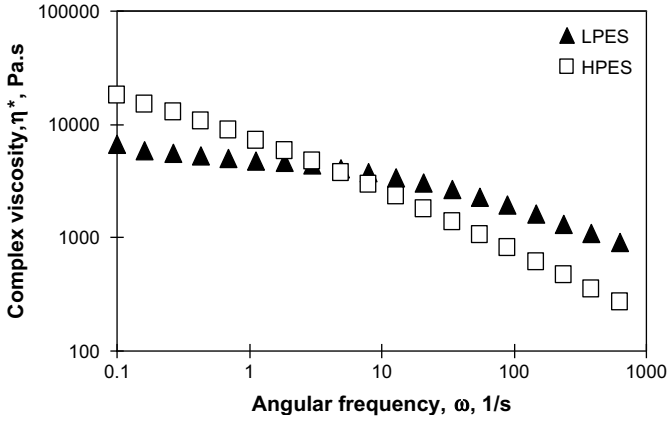

Fig. 4. Dynamic frequency sweep tests for LPES and HPES polymer melts with complex viscosity at their linear viscoelastic range (10% strain applied).

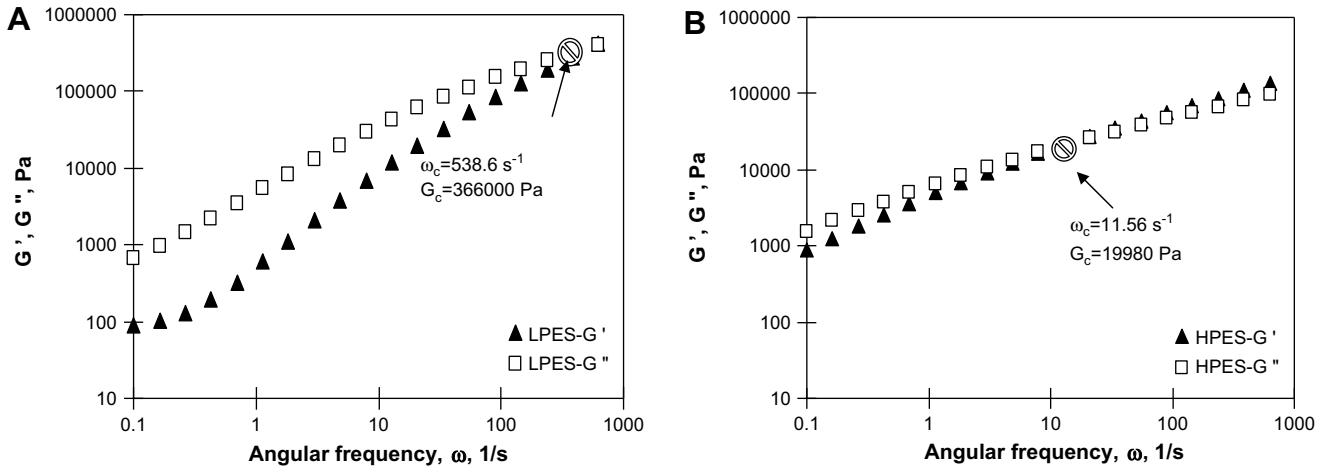

Fig. 5. Dynamic frequency sweep tests of (A) LPES and (B) HPES polymer melts with storage and loss moduli (10% strain applied).

3. Results and discussion

3.1. Thermal properties of HPES and LPES materials

Table 2 summarizes the basic thermal properties, molecular weights and rheological properties of HPES and LPES materials. The TGA results show that HPES is more thermally stable with a higher T_d value (579.72 °C) than LPES (526.85 °C), which is mainly due to the branched polymer's globular and compact structure [23]. Fig. 3 shows the T_gs measured by DMA for dense films cast from these two polymers where the loss tangent (tan δ) peak temperature is chosen as the T_g [24]. For both polymers, their storage moduli display a slow decline between −80 °C and 200 °C, indicating a low energy molecular relaxation. Corresponding peaks in their loss moduli are similarly produced at around −60 °C (γ transition), 70 °C (β transition), and 230 °C (α transition): As the LPES and HPES materials warm and expand, their free volume increases so that localized bond movements by bending, stretching and side chain movements may occur [25]. The T_gs identified by the tan δ peaks for both polymer analogues are quite similar with less than 3% difference. This can be explained by their same functional groups in the polymeric matrix.

3.2. Rheological characterization of HPES and LPES melts

Fig. 4 shows the complex viscosities of LPES and HPES melts against the applied dynamic angular frequency. For LPES melts, a viscosity plateau, the so-called Newtonian plateau can be observed at low enough angular frequencies, whereas the complex viscosity curve of HPES melts deviates from the ideal plateau at the low frequency range and shows a higher viscosity compared to its linear analogue. This is most probably due to its branched macromolecular structure because the side chains may bring more pronounced shear thinning behavior. For LPES, the zero-shear viscosity at 370 °C was extrapolated with 5650 Pa s using the Carreau–Yasuda regression method. This regression is suitable for polymers with zero-shear viscosity and Power Law region. Nevertheless, for HPES no zero-shear viscosity could be found as it is a densely branched material. Table 2 summarizes the Carreau–Yasuda regression results obtained from the master curves of LPES and HPES melts and indicates that the HPES material possesses a significant longer relaxation time and a narrower Newtonian to Non-Newtonian transition.

The dynamic frequency tests for both polymer melts at 10% strain with storage modulus (G') and loss modulus (G'') are shown in Fig. 5-A and -B. For LPES melt in the range of Newtonian Plateau (angular frequency from 0.1 to 1 s^{-1}), the slope of its loss modulus curve in the double logarithmic plot is equal to one, while the slope of its storage modulus curve is equal to two. However, for HPES melt, the slopes of its loss and storage modulus curves are quite close, indicating more viscoelastic nature.

The storage moduli G's of both melts at low frequencies are lower than G''s, implying that the rheology at low frequencies is mainly influenced by viscous portion. By increasing the frequency, the so-called crossover point (COP) between G' and G'' occurs, indicating a transition from a more viscous-like deformation behavior to a more elastic one. Therefore, COP is a criterion for melt viscoelastic characterization and its value can provide qualitative information about material's average molecular weight (M_w), degree of branching and molecular mass distribution (MMD).

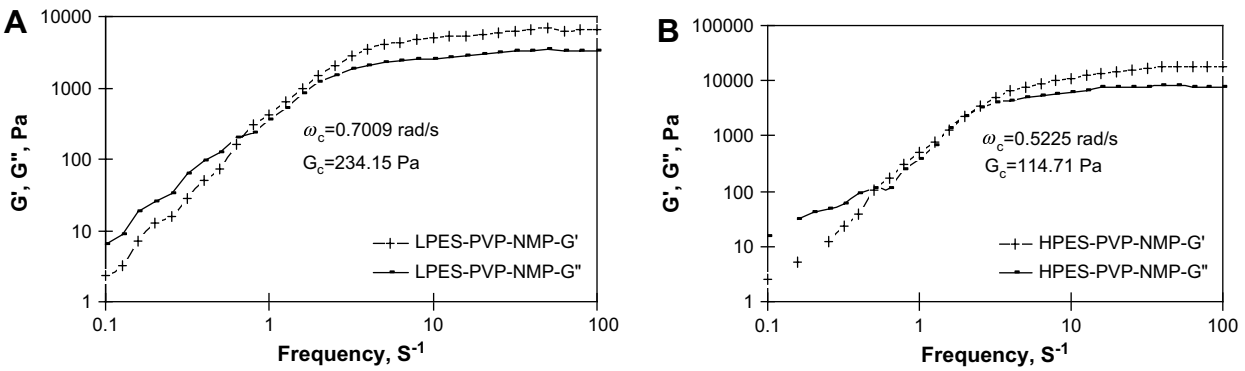

Fig. 6. Dynamic frequency sweep tests of (A) 16/10/74 wt% LPES/PVP/NMP and (B) 16/10/74 wt% HPES/PVP/NMP ternary dope solutions at 1% strain.

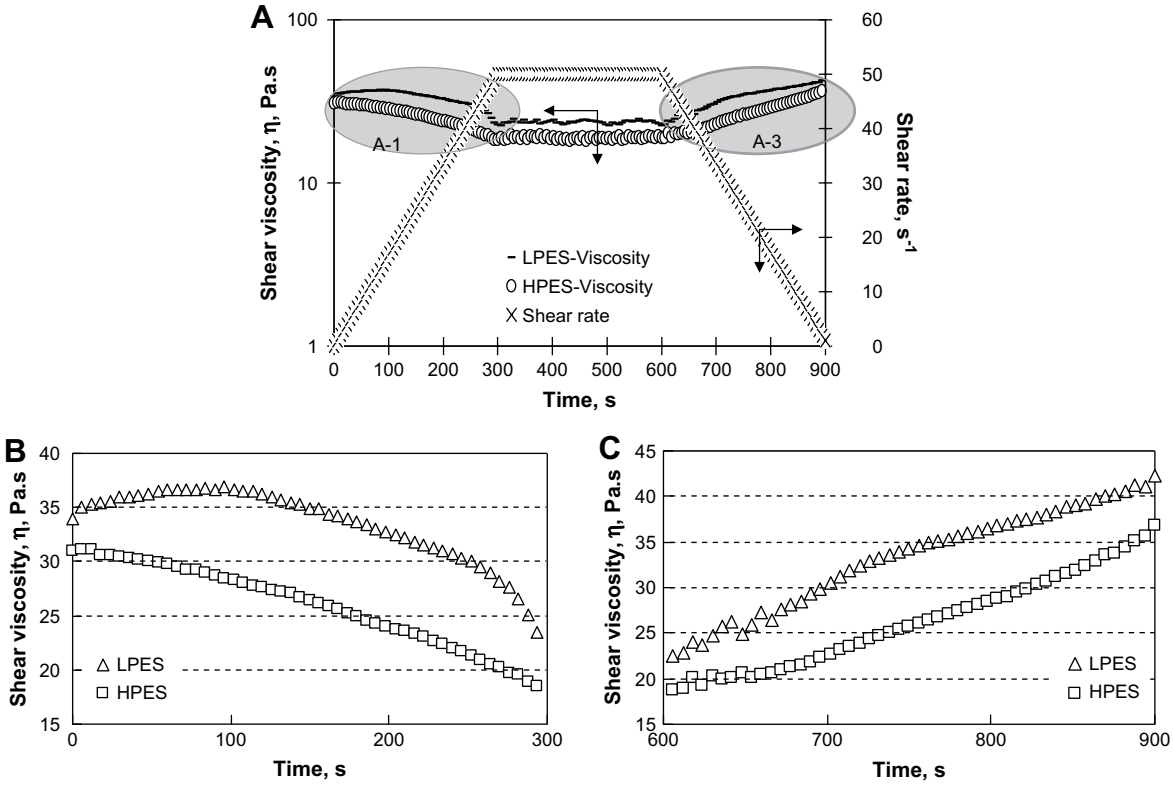

Fig. 7. The time dependent flow behavior for both LPES and HPES ternary dope systems with (A) loop shear rate; (B) viscosity changes under shear; (C) viscosity recovery upon relaxation.

The COP shift to a lower angular frequency (i.e., $\omega_c = 11.56\ s^{-1}$ for HPES vs. $\omega_c = 538.6\ s^{-1}$ for LPES) is caused by an increase in average molecular weight or branching structure for the HPES material. This can be easily understood that even at higher frequencies shorter molecules remain mobile, whereas longer or more branched molecules become immobile at lower angular frequencies. A vertical shift of the COP towards a lower modulus for HPES melts ($G_c = 19{,}980$ Pa) indicates a wider molecular mass distribution (MMD). The wider MMD could be attributed to the interactions of polymer side chains or branches in HPES macromolecules. The quantitative data for materials' molecular weight (M_w) and polydispersity index (PDI) obtained via sophisticated molar mass distribution (MMD) method [26–28] are tabulated in Table 2 and are in consistent with our qualitative interpretations. It should be noted that usually the rheo-MMD conversion is based on the rheological theory for linear chain polymers only. As there is no general model available for branched polymers or in general for technical polymers the values can only be used for a relatively qualitative comparison between both linear and branched samples.

3.3. The rheology of polymer dope solutions and its influence on membrane formation

The rheological properties of polymer dope solutions play a paramount role in determining membrane morphology and separation performance. Similar to the molten PES samples, the dynamic frequency tests of the LPES/PVP/NMP and HPES/PVP/NMP ternary polymeric solutions at 1% strain at room temperature show that the COP of HPES dope ($\omega_c = 0.5225$ rad/s and $G_c = 114.71$ Pa) has lower frequency and shear modulus than those for LPES dope ($\omega_c = 0.7009$ rad/s and $G_c = 234.15$ Pa) (refer Fig. 6-A and -B). Fundamentally, the frequency (ω_c) at the COP is related to a characteristic relaxation time (τ_c) of a polymeric dope as follows [17]:

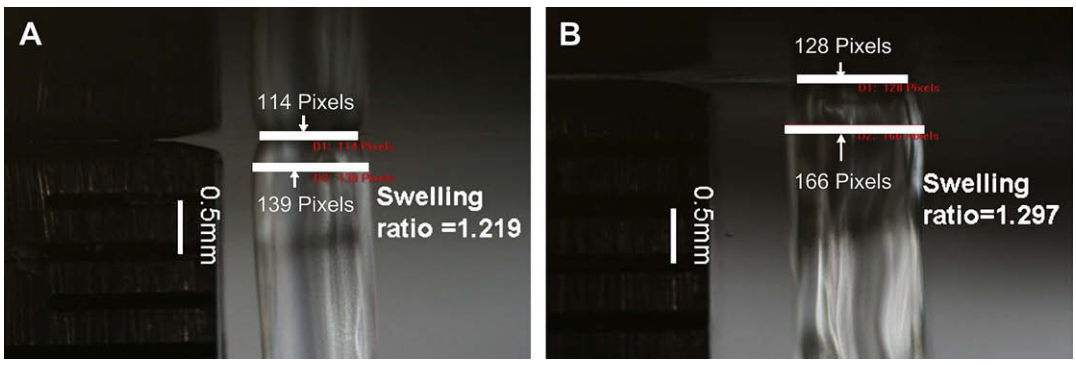

Fig. 8. Typical die swell images for hollow fiber membrane formations via (A) LPES/PVP/NMP 16/10/7 wt% and (B) HPES/PVP/NMP 16/10/74 wt% polymer dopes by dry-jet wet spinning.

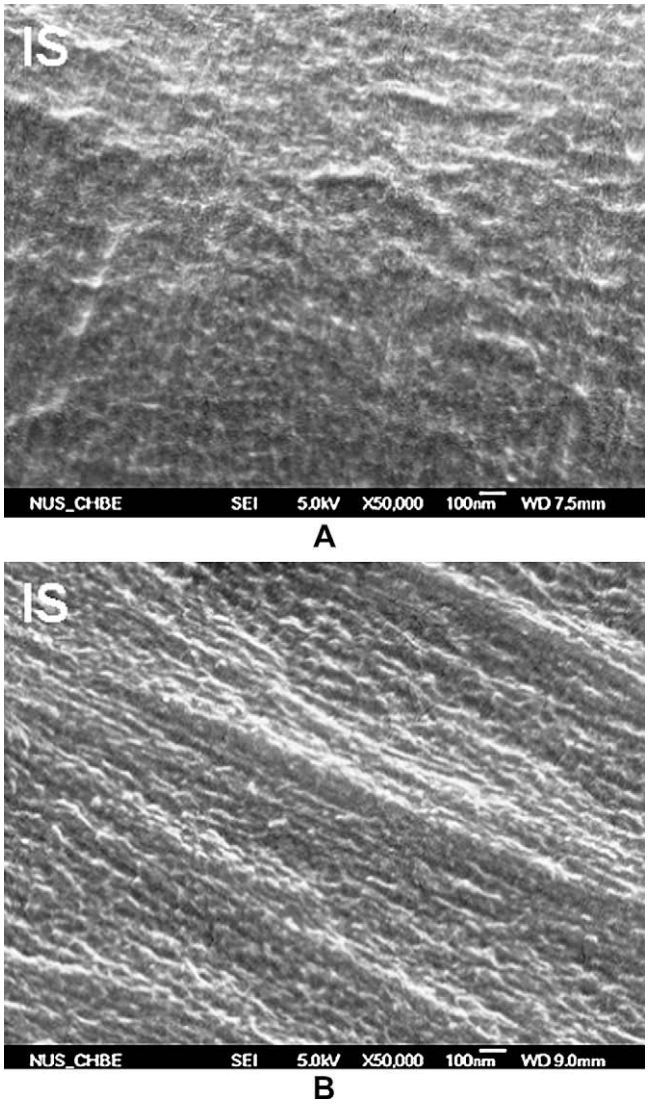

Fig. 9. Inner-surface SEM images of (A) LPES and (B) HPES hollow fiber membranes.

Table 3
Summary of ultrafiltration and mechanical test results for as-spun LPES and HPES hollow fiber membranes.

Mem. ID	Ultrafiltration results			Mechanical test results	
	μ_p (nm)	PWP (L/m^2/bar/h)	MWCO (Da)	Break strength (Pa)	Load at break (N)
LPES	2.86	5.43	8421	3.19 ± 0.42	1.41 ± 0.18
HPES	2.51	6.65	5612	2.81 ± 0.24	1.25 ± 0.11

$$\tau_c = \frac{2\pi}{\omega_c} \tag{5}$$

As a result, the characteristic relaxation time of the LPES ternary dope solution ($\tau_c = 8.96$ s) is shorter than that of HPES ($\tau_c = 12.02$ s). A higher τ_c indicates a greater memory for the HPES polymer solution system and it would take a longer time for HPES polymeric chains to relax and return to their original states after experiencing strains.

Thixotropy tests, the time dependent flow behaviors for both polymer ternary systems are shown in Fig. 7. It shows that for both polymeric fluid systems, their shear viscosity changes with a progressively increased shear rate are similar to the complex viscosity changes of their corresponding molten materials over increased angular frequencies (refer Fig. 4): LPES shows a Newtonian fluid behavior at low enough angular frequencies, whereas HPES shows more pronounced shear thinning and faster transition from Newtonian to Non-Newtonian flow behavior. The relaxation performances for both polymer solutions under a progressively decreased shear rate are shown in Fig. 7-C. It indicates that it takes a longer time of around 250 s for the HPES polymer solution to resume its original viscosity ($\sim$31 Pa s), whereas for LPES it takes only around 200 s to return to its plateau viscosity ($\sim$36 Pa s). The rheology studies based on the polymeric solutions also reveal that the branching structure of HPES provides it a narrower Newtonian to Non-Newtonian transition and a higher relaxation time. Notice should be taken that the higher viscosities for both polymer solutions in the end of thixotropy tests relative to their original values are probably due to the evaporation of the solvent during an extended period of 15 min tests.

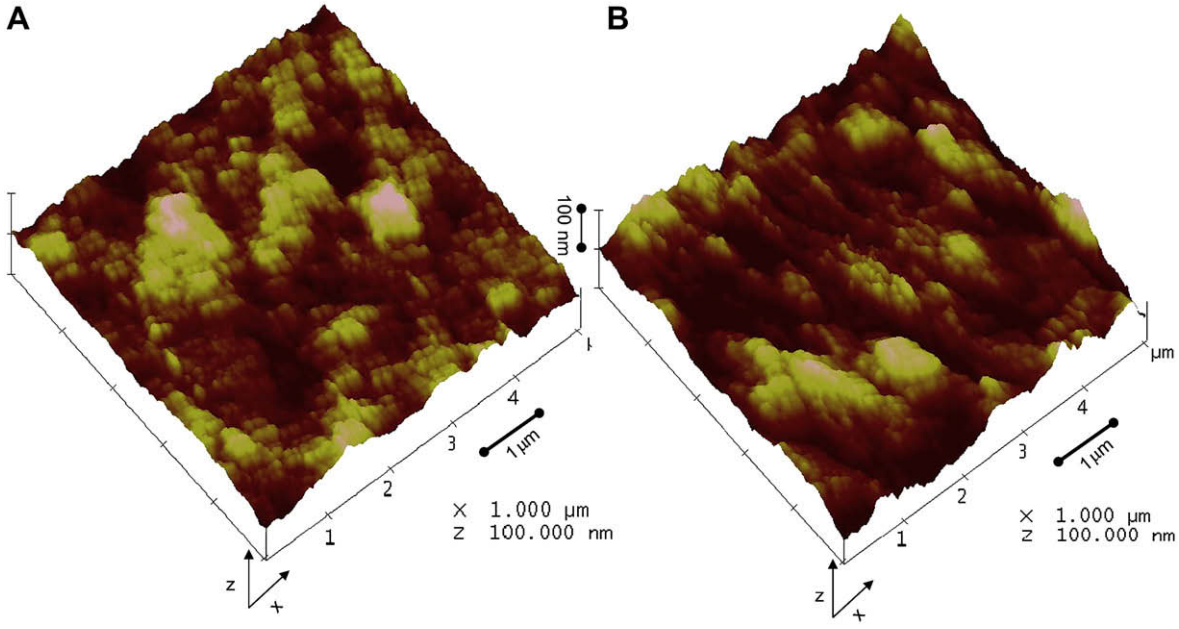

Fig. 10. Inner-surface AFM images of the (A) LPES and (B) HPES hollow fiber membranes.

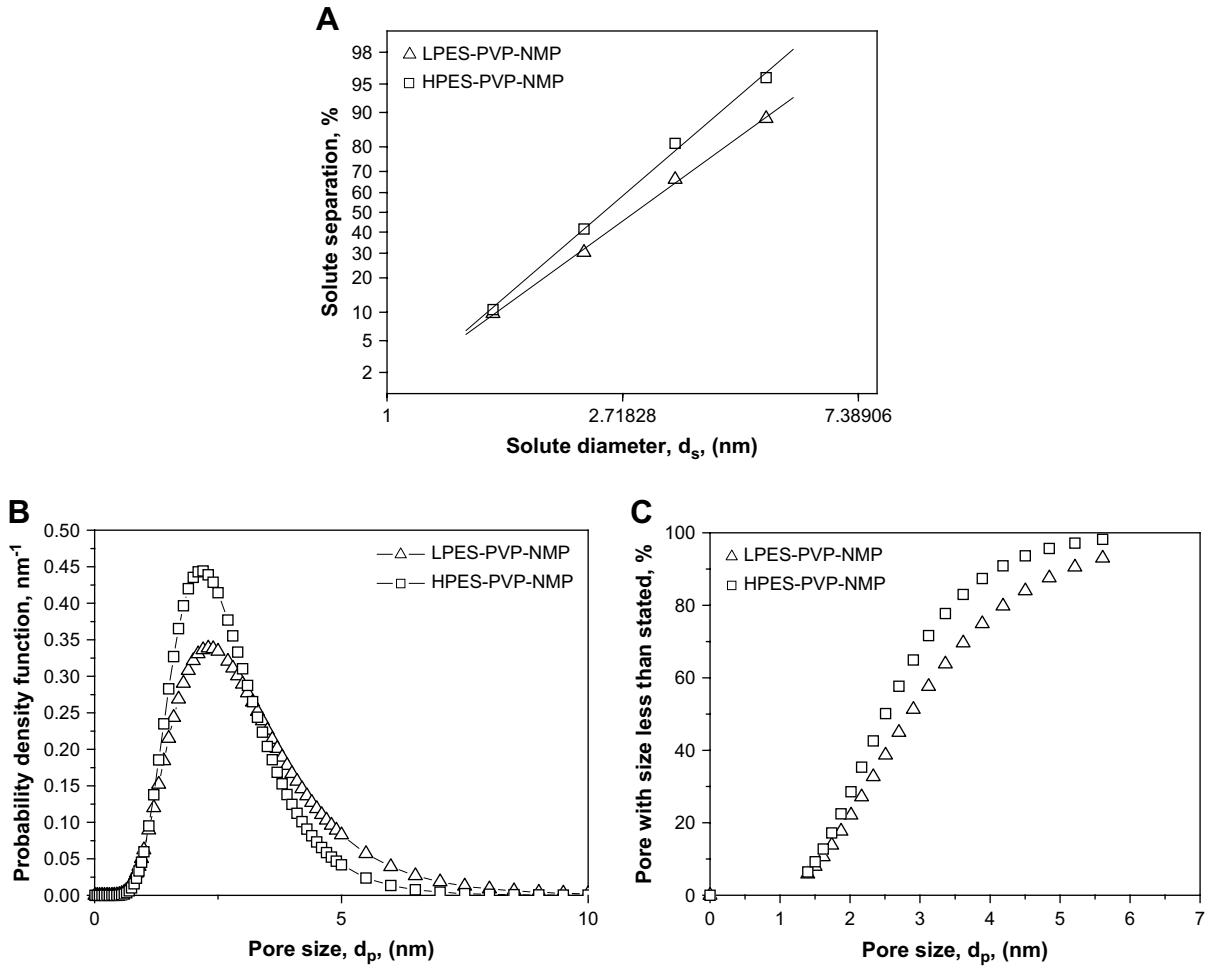

Fig. 11. (A) Solute separation curve; (B) probability density function curve; (C) cumulative pore size distribution curve for as-spun LPES and HPES hollow fiber membranes.

Fig. 8 shows the typical die swell phenomenon during the hollow fiber formation via dry-jet wet spinning process. The die swell can be considered as a consequence of memory effects of polymer materials that have been investigated both experimentally and theoretically by many researchers [29–32]. The extrudate swell through a short channel depends on both the material characteristics (molecular weight, molecular weight distribution and viscoelasticity) and the die geometry. The shear stress may lead to the disentanglement and orientation of macromolecular random coil chains in the spinneret's capillary channel. As shown in Fig. 8, the HPES has a larger die swelling because of possessing higher entanglement density and a higher normal stress [33]. The slower relaxation development in the HPES nascent fiber could be explained by its slower relaxation development after leaving the spinneret due to its higher memory, longer chain re-entanglement time or longer characteristic relaxation time.

On the other hand, the significantly higher relaxation time for HPES indicates that it should take a longer time to return to its original ball-shaped random coil chains when it is extruded through the spinneret in the dry-jet wet spinning process. Taken into considerations of our previous findings of the almost same phase separation thermodynamics and kinetics for linear and hyperbranched polymer systems [15], the less relaxation of HPES in the hollow fiber spinning process may result in more oriented morphology with elliptical pores rather than round pores. A comparison of SEM pictures of the inner-surface pore structures of LPES and HPES hollow fibers, as illustrated in Fig. 9, clearly shows that the HPES hollow fiber holds elliptical or slit pores. It should be noted that the selective skins for both membranes are located in their inner surface. A similar conclusion can be observed from the AFM study with tapping mode, as displayed in Fig. 10, where the HPES hollow fiber has elliptical or slit pores, while the LPES has round pores.

In addition, the ultrafiltration characterization results in Table 3 and the pore size distributions for LPES and HPES hollow fiber membranes in Fig. 11 provide additional data supporting our hypothesis: The as-spun HPES hollow fiber has smaller pore sizes

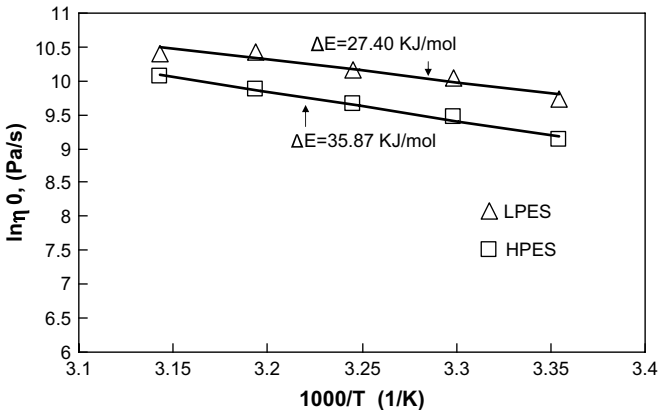

Fig. 12. Arrhenius plots of zero-shear viscosity for 16/10/74 wt% polymer/PVP/NMP dope solutions.

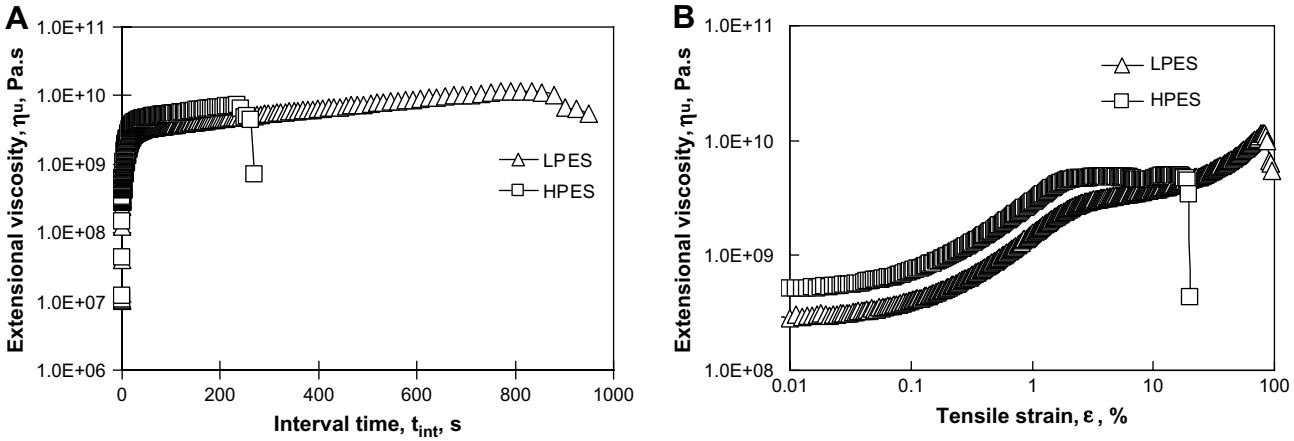

Fig. 13. Extensional viscosity measurements for LPES and HPES melts (A) over the time and (B) over the tensile strain.

and narrower pore size distribution than the LPES one. The former also has a higher rejection rate than the latter for the same solutes.

To further explore the temperature dependence of both polymer dope solutions, the zero-shear viscosity determined by equation (3) is plotted against the reciprocal temperature in Fig. 12. The good linear fit for both polymer dope solutions indicates that their zero-shear viscosity follows the Arrhenius relationship with activation energies of 27.40 kJ/mol for LPES solutions and 35.87 kJ/mol for HPES solutions.

3.4. The mechanical properties of LPES and HPES materials

The measurement of extensional viscosity is a very sensitive method for distinguishing polymer materials with different degrees of branching, whereas traditional shear tests using rotational or capillary rheometer are not able to detect these changes [34]. The extensional viscosity results reveal that the LPES asymmetric film is more resistant to high tensile strains. In contrast, the HPES asymmetric film breaks faster (Fig. 13-A) and easier (Fig. 13-B) which could be related to its so-called more "strain hardening effect" due to its branching structure with more side chains. Our results are in line with the elongation evaluation of high-density polyethylene (HDPE) with different branching degree [34]. Generally a material deforms elastically for small deforming forces but returns to its original shape when the deforming force is removed. However for HPES films the relatively lower deforming force applied beyond its elastic limit could disable its resumption even when the force is removed: it deforms plastically. The qualitative Instron data for hollow fibers spun with these two materials in Table 3 also reveal that HPES fiber is more mechanically weak due to its intrinsic branching structure.

4. Conclusions

Comprehensive explorations of the rheological properties of linear and hyperbranched polyethersulfone materials were conducted to identify the intrinsic causes for their differences on macromolecular structure and processability in hollow fiber spinning. The following conclusions can be summarized:

1. The rheological studies on the molten HPES and LPES materials show that HPES has a larger molecular weight and a wider molecular weight distribution compared to its linear analogue.
2. The polymeric solutions' rheological behaviors reveal that the HPES dope solution has a longer relaxation time than its linear counterpart. Hence the HPES nascent fiber shows a more pronounced die swell occurring at the spinneret exit. In addition, the slower chain re-entanglement and slower chain relaxation lead the HPES as-spun hollow fiber membrane with smaller pore sizes, narrower pore size distribution, and a smaller molecular weight cut-off (MWCO).
3. The extensional viscosity characterizations show that HPES has a more strain hardening effect due to its branched structure. As a result, the HPES asymmetric film breaks more easily under high extensional strain and HPES hollow fiber has a weaker mechanical strength.

Acknowledgements

The authors would like to thank BASF Company, Germany for funding this research project with a grant number of R-279-000-188-592. Thanks are also going to the NUS grant of R-279-000-249-646 for the initiative on advanced membranes for pharmaceutical and biomedical applications. We also highly appreciate Institute of Material Research and Engineering (IMRE), Singapore for providing DMA measurements.

References

[1] Barzin J, Madaeni SS, Mirzadeh H, Mehrabzadeh M. J Appl Polym Sci 2004;92:3804–13.
[2] Barzin J, Feng C, Khulbe KC, Matsuura T, Madaeni SS, Mirzadeh H. J Membr Sci 2004;237:77–85.
[3] Sakai K. J Chem Eng Jpn 1997;30:587–99.
[4] Kim YH. J Polym Sci Part A Polym Chem 1998;36:1685–98.
[5] Voit B. J Polym Sci Part A Polym Chem 2000;38:2505–25.
[6] Turner SR, Voit BI. Polym News 1997;22:197–202.
[7] Gao C, Yan D. Prog Polym Sci 2004;29:183–275.
[8] Kwak SY, Ahn DU. Macromolecules 2000;33:7557–63.
[9] Cox WP, Merz EH. J Polym Sci 1958;28:619–22.
[10] Alhadithi TSR, Barnes HA, Walters K. Colloid Polym Sci 1992;270:40–6.
[11] Kulicke WM, Porter RS. Rheol Acta 1980;19:601–5.
[12] Khanna YP. Polym Eng Sci 1991;31:440–4.
[13] Bair S, Qureshi F. J Tribol-T ASME 2003;125:70–5.
[14] Yang Q, Chung TS, Santoso YE. J Membr Sci 2007;290:153–63.
[15] Yang Q, Chung TS, Chen SB, Weber M. J Membr Sci 2008;313:190–8.
[16] Larson GL. The structure and rheology of complex fluids. New York: Oxford University Press; 1999.
[17] Bai DS, Khin CC, Chen SB, Tsai CC, Chen BH. J Phys Chem B 2005;109:4909–16.
[18] Gholami M, Nasseri S, Feng CY, Matsuura T, Khulbe KC. Desalination 2003;155:293–301.
[19] Wang KY, Matsuura T, Chung TS, Guo WF. J Membr Sci 2004;240:67–79.
[20] Youm KH, Kim WS. J Chem Eng Jpn 1991;24:1–7.
[21] Singh S, Khulbe KC, Matsuura T, Ramamurthy P. J Membr Sci 1998;142:111–27.
[22] Rafat M, De D, Khulbe KC, Nguyen T, Matsuura T. J Appl Polym Sci 2006;101:4386–400.
[23] Borah J, Mahapatra SS, Saikia D, Karak N. Polym Degrad Stab 2006;91:2911–6.
[24] Foreman S, Sauerbrunn SR, Marcozzi CL. Exploring the sensitivity of thermal analysis techniques to the glass transition. Thermal Analysis & Rheology, Application note number TA-082B. TA Instruments, Inc. http://www.tainst.com.

[25] Menard K. Dynamic mechanical analysis: a practical introduction. Boca Raton: CRC Press; 1999.
[26] Braun H, Eckstein A, Fuchs K, Friedrich C. Appl Rheol 1996;6:116–23.
[27] Mead DW. J Rheol 1994;38:1797–827.
[28] Thimm W, Friedrich C, Maier D, Marth M, Honerkamp J. Appl Rheol 1999;9:150–7.
[29] Su Y, Lipscomb GG, Balasubramanian H, Lloyd DR. AIChE J 2006;52:2072–8.
[30] Yang XT, Xu ZL, Wei YM. J Appl Polym Sci 2006;100:2067–74.
[31] De Rovere A, Shambaugh RL. Polym Eng Sci 2001;41:1206–19.
[32] Oh TH, Lee MS, Kim SY, Shim HJ. J Appl Polym Sci 1998;68:1209–17.
[33] Rwei SP. J Appl Polym Sci 2001;82:2896–902.
[34] Franck A. Extensional viscosity of polyolefin and polystyrene. Technical note number AAN020. TA Instruments.